

A Bayesian Approach to Constraining Cosmological Parameters using Planck Public Data II

MATTIAS LAZDA¹

¹ McGill University
3600 Rue University,
Montréal, QC H3A 2T8

ABSTRACT

Ever since the Cosmic Microwave Background (CMB) was detected in 1965 by Arno Penzias and Robert Wilson, astrophysicsts have continuously aimed to gain a better understanding of the origin the CMB. To this day, studies of the anisotropies observable within the CMB continue to be of particular interest as they provide a window into the fundamental physics that dictate the expansion of our early universe. Using the publicly available data from the Planck Public Data II release of the CMB power spectrum, we constrain six fundamental cosmological parameters ($A_s, n_s, \tau, \Omega_b h^2, \Omega_c h^2, H_0$) through Markov Chain Monte Carlo simulations. We compare the effects of using a Gaussian likelihood versus a Lorentzian likelihood in our simulations and determine that the Gaussian likelihood is slightly favoured with both yielding nearly identical best fits with $\chi^2_\nu = 1.026$ (Gaussian) and $\chi^2_\nu = 1.027$ (Lorentzian).

Keywords: Markov Chain Monte Carlo — Cosmic Microwave Background

1. INTRODUCTION

In the beginning, there was a bang. Some would even call it a Big Bang. In mere fractions of a second, our universe evolved from a tiny, dense ball of energy into an ever expanding universe which – to this day – continues to expand. In its early stages of its life, the temperature of our universe was so hot that space was composed of hot plasma: as much as atoms wanted to form, constituent particles simply had too much energy to form stable bonds with one another. However, as our universe continued to expand, its temperature began to drop, and as our universe approached its roughly 400,000th birthday, the temperature dropped just enough for the first atoms to form. This is known as the *Epoch of Recombination*.

1.1. The Cosmic Microwave Background

Prior to recombination, the hot plasma with its high opacity prohibited photons from being able to escape its hot, excited medium. However, once atoms could form for the first time, leftover photons suddenly had plenty of room to freely travel through space at their own will. This “leftover” radiation that exited at recombination is known as the Cosmic Microwave Background (CMB), providing us with a snapshot of how our universe looked like roughly 400,000 years after the Big Bang.

Recall that a blackbody can be modelled by Planck’s law of black body radiation(Kramm & Mölders 2009):

$$B_\nu(T) = \frac{2h\nu^3}{c^2} \frac{1}{\exp\left(\frac{h\nu}{kT}\right) - 1}, \quad (1)$$

where T is the temperature of the blackbody peaking at frequency ν , and c, h and k are the speed of light, Planck's constant and Boltzmann's constant, respectively. When observing our universe, regardless of the direction we look in, we see a black body spectrum with $T = 2.725\text{K}$ (Noterdaeme et al. 2011), peaking at a frequency in the microwave regime of the electromagnetic spectrum. To first order, the CMB is a perfect black body. However, as we look closer, we start to notice small differences in the spectrum. These *anisotropies* were first mapped by the Cosmic Background Explorer (COBE) mission, whose goal was to probe the CMB. They were later improved in 2006 with the Wilkinson Microwave Anisotropy Probe (WMAP) mission and again in 2013 with the Planck telescope. A comparison of the measured anisotropies is provided in Figure 1.

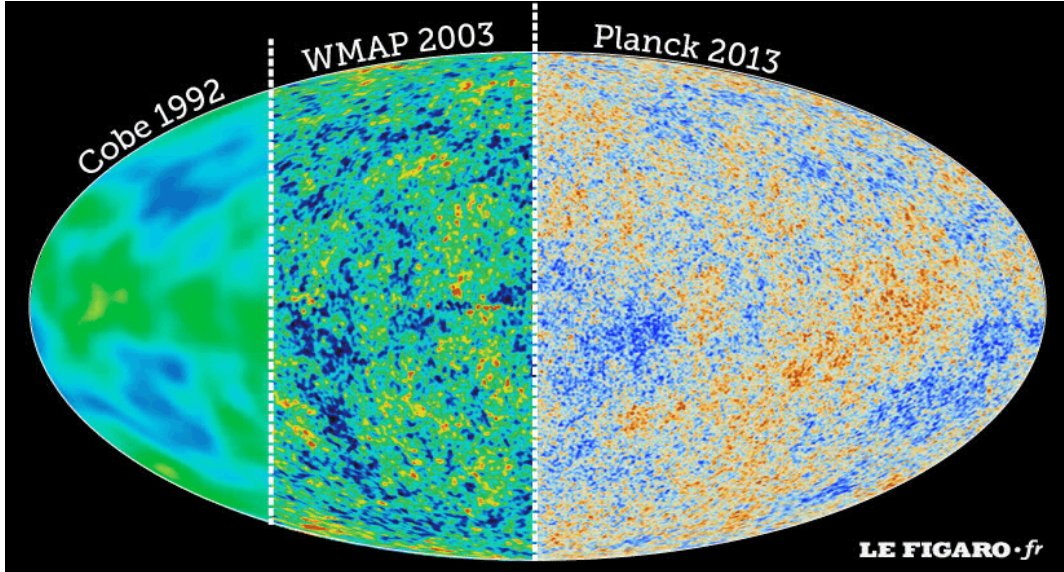


Figure 1. Comparison of the anisotropies measured by the COBE, WMAP and Planck mission respectively. Resolution has significantly improved over the course of two decades, allowing for better probing of the CMB power spectrum and further constraint of the fundamental cosmological parameters that govern our universe. Image retrieved from [here](#).

1.2. Baryonic Acoustic Oscillations

In the early universe, the primordial plasma can be understood as a fluid known as the *photon-baryon* fluid. Within this fluid, regions of slightly higher density would collapse towards one another due to gravity: however, radiation pressure would act as a restoring force, pushing outwards away from the regions of high density. Together, this push and pull formed propagating waves known as *baryonic acoustic oscillations*. These oscillations in our early Universe lead to a characteristic acoustic scale in the CMB which tell us how far a wave in the photon-baryon fluid can actually travel, giving us insight into the geometry of our universe.

1.3. The CMB Power Spectra

Much of the physics of the CMB is driven by BAOs so to understand the CMB, we must better understand the BAOs. To distinguish the different contributions that make up the BAOs, we take our usual approach of using Fourier transforms. However, given that the function we are trying to decompose lives on a sphere rather than a cartesian axis, we require spherical harmonics which depend on angular position (θ, ϕ) .

Decomposing our map of the sky into spherical harmonics yields functions of the form

$$Y_{\ell m}(\theta, \phi), \quad (2)$$

where ℓ is akin to the wavenumber in one-dimensional Fourier space (e.g. large ℓ modes correspond to small scales) and m controls the orientation of the sinusoids. We can then write the temperature of the sky as a function of the spherical harmonics:

$$T(\theta, \phi) = \sum_{\ell, m} a_{\ell m} Y_{\ell m}(\theta, \phi), \quad (3)$$

where $a_{\ell m}$ scales the contributions of each of the $Y_{\ell m}$'s. In the same vein as solving for Fourier coefficients, we find that

$$a_{\ell m} = \int d\Omega Y_{\ell m}^*(\theta, \phi) T(\theta, \phi), \quad (4)$$

where we integrate over all angular limits. From this, we compute the angular power spectrum:

$$\hat{C}_\ell = \frac{1}{2\ell + 1} \sum_{m=-\ell}^{+\ell} |a_{\ell m}|^2, \quad (5)$$

where we average over m since the universe has no preferred orientation. This angular power spectrum differentiates between the amount of small-scale power versus large-scale power in a map and is something we can aim to measure.

1.4. Planck Public Data II

In 2015, the entire data obtained by the Planck telescope from 2009 – 2013 was made publicly available. From the data, one could easily obtain measurements of CMB power spectra. The CMB power spectra is provided in Figure 2. Only some errorbars on the measurements are included to not crowd the entire image.

To successfully model the CMB power spectra, one must constrain six parameters, each impacting the CMB power spectra in varying ways. In this report, we model the CMB following the model utilized in [Fendt & Wandelt \(2007\)](#), which is described in more detail in [2](#). In short, the six parameters are n_s , the primordial tilt of the power spectrum; τ , the optical depth to scattering; $\Omega_b h^2$, the fractional baryon density; $\Omega_c h^2$, the fractional cool dark matter density; H_0 , the Hubble parameter and A_s , the primordial amplitude of the spectrum, where $h = \frac{H_0}{100 \frac{\text{km}}{\text{s Mpc}}}$. In this report, we aim to use Markov Chain Monte Carlo (MCMC) simulations to constrain these six basic cosmological parameters.

The report is structured as follows. In [§2](#), we discuss the package used to simulate our CMB power spectra maps. In [§3](#), we employ the use of MCMC to constrain the basic cosmological parameters, followed by the results and discussion of the results in [§4](#). Lastly, we summarize our work in [§5](#).

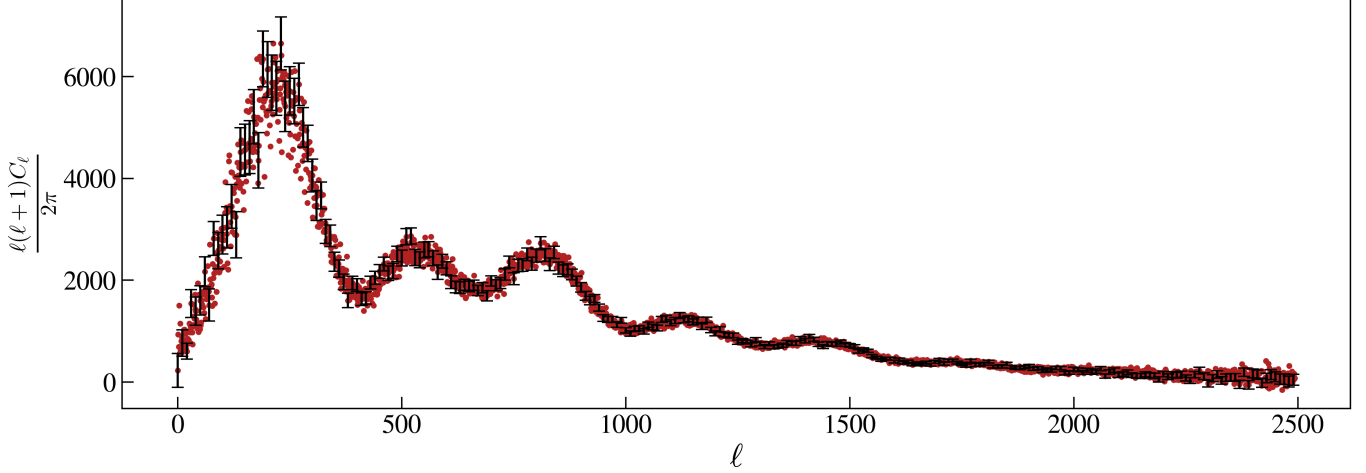


Figure 2. CMB power spectrum measured by the Planck telescope. Only some errorbars are included to not overcrowd the image. Vertical axis represents the angular power spectrum, C_ℓ up to multiplicative constant as a function of ℓ which is akin to the wavenumber in one-dimensional Fourier space.

2. PICO

Pico, short for Parameters for Impatient Cosmologists, is a software which computes the CMB power as a function of the cosmological parameters mentioned above by interpolating through precomputed training data (Fendt & Wandelt 2007). Briefly, a set of N vectors of cosmological parameters $\mathbf{x}^{(j)}$ with dimension \mathcal{N}_x and corresponding power spectrum $\mathbf{y}^{(j)}$ with dimension \mathcal{N}_y are embedded into a $(\mathcal{N}_x + \mathcal{N}_y)$ -dimensional Euclidean space. The k th component of \mathbf{y} is then approximated as a p th order polynomial dependent on \mathcal{N}_x given by:

$$y_k = \sum_{i_1 \geq i_2 \geq \dots \geq i_p}^{\mathcal{N}_x} \alpha_{i_1 i_2 \dots i_p} x_{i_1} x_{i_2} \dots x_{i_p}, \quad (6)$$

where $\alpha_{i_1 i_2 \dots i_p}$ are chosen to minimize the squared error over the training set provided in Fendt & Wandelt (2007), Appendix A. This is then converted into a matrix equation, allowing for extremely quick computations of the CMB power spectra given a set of input parameters $\mathbf{x}^{(j)}$, the same one's we defined previously. For more details on the algorithm, see Fendt & Wandelt (2007). Although this will be unable to provide the most accurate results possible, the output is sufficient for the purposes and goals of this experiment, which is to show the viability of using MCMC to estimate the basic cosmological parameters governing the CMB power spectra.

3. MARKOV CHAINS MONTE CARLO

Recall that given a prior belief that a probability distribution function is $p(A_s, n_s, \tau, \Omega_b h^2, \Omega_c h^2, H_0)$ and that our observations of the CMB power spectra have a likelihood $p(y_i | A_s, n_s, \tau, \Omega_b h^2, \Omega_c h^2, H_0)$ of occurring, Baye's theorem tells us that the posterior probability is proportional to

$$p(A_s, n_s, \tau, \Omega_b h^2, \Omega_c h^2, H_0 | y_i) \propto p(y_i | A_s, n_s, \tau, \Omega_b h^2, \Omega_c h^2, H_0) \times p(A_s, n_s, \tau, \Omega_b h^2, \Omega_c h^2, H_0). \quad (7)$$

Markov chain Monte Carlo (MCMC) is a set of algorithms for sampling from the probability distribution given in Eq. (7), determining the most likely values of the model parameters. To successfully

carry out MCMC, we require specifying the prior on our input parameters as well as the likelihood function that governs the output of the CMB power spectra, C_l . Combined, these form a posterior distribution of our model parameters. According to Eq. (5), the output is a squared quantity. Consequently, we expect that the likelihood that best models this data is something that is strictly positive. However, given that there is not a simple closed analytic form for the real likelihood, we will test both a Gaussian likelihood as well as a Lorentzian likelihood, which do allow for negative values. A more in depth description of these likelihoods follows.

3.1. Estimating the Prior on our Cosmological Parameters

Before we cover the likelihoods, we require specifying a prior for each of the six parameters discussed in §1.4. Our goal was to avoid introducing any bias into any of the priors (e.g. that $H_0 \sim 68 \text{ km}\cdot\text{s}^{-1}\cdot\text{Mpc}^{-1}$). We noticed that if we provided Pico a trial parameter that is outside the physical range set by Pico (for example, a negative H_0), it would be unable to interpolate through the trial data and thus unable to give an output CMB power spectrum. Consequently, we simply let Pico dictate the prior on the parameters. Although this adds inherent bias to the resulting posterior distribution, it was the most general form that we could obtain and the effects were only noticeable in a small portion of the results.

3.2. Gaussian Likelihood

The first likelihood function sampled was the Gaussian likelihood, described algebraically by

$$\mathcal{L}_G = p(y_i|A_s, n_s, \tau, \Omega_b h^2, \Omega_c h^2, H_0) = \prod_i^N \frac{1}{\sqrt{2\pi\sigma_i^2}} \exp\left[-\frac{(y_i - f(x, A_s, n_s, \tau, \Omega_b h^2, \Omega_c h^2, H_0))^2}{2\sigma_i^2}\right]. \quad (8)$$

Here, f is the model function computed by Pico dependent on the input parameters and σ_i are errorbars on the y_i th data point, assumed to be Gaussian. Taking the log of the above expression yields the Gaussian log likelihood, given by

$$\log\mathcal{L}_G = -\frac{1}{2} \sum_{i=1}^N \left(\frac{(y_i - f_i(x, A_s, n_s, \tau, \Omega_b h^2, \Omega_c h^2, H_0))^2}{\sigma_i^2} + \log(\sigma_i^2) \right). \quad (9)$$

Note that the reason for specifying the log-likelihood is because the MCMC algorithm that was used, `emcee` (Foreman-Mackey et al. 2013), requires the log likelihood.

3.3. Lorentzian Likelihood

The second likelihood sampled was the Lorentzian likelihood, expressed algebraically as

$$\mathcal{L}_L = \prod_{i=1}^N \frac{1}{\pi} \left[\frac{\frac{1}{2}\Gamma_i}{(y_i - f_i(A_s, n_s, \tau, \Omega_b h^2, \Omega_c h^2, H_0))^2 + \frac{\Gamma_i^2}{4}} \right], \quad (10)$$

where Γ is the Full Width Half Maximum (FWHM) of the model Lorentzian. Assuming Gaussianity on the errorbars, we can relate the FWHM to the errorbars by

$$\Gamma_i = 2\sqrt{2\log 2}\sigma_i, \quad (11)$$

obtained by solving for the width of a Gaussian at half maximum. The log likelihood in this case is simply

$$\log \mathcal{L}_L = \sum_{i=1}^N \left[-\log \left((y_i - f_i(A_s, n_s, \tau, \Omega_b h^2, \Omega_c h^2, H_0))^2 + \frac{\Gamma_i^2}{4} \right) + \log \left(\frac{\Gamma_i^2}{4} \right) \right]. \quad (12)$$

Given this, we now had two probability density functions to sample from with our MCMC.

4. RESULTS

To carry out the MCMC algorithm, we employed the use of `emcee` (Foreman-Mackey et al. 2013), a python package designed for sampling varying log likelihoods. Sampling 10,000 steps with 50 walkers and removing the first 1000 sampled data points to remove the burn in period, we obtained the resulting posterior distributions for all of the model parameters. Figure 3 provides the resulting posterior distributions obtained from the Gaussian likelihood whereas Figure 4 is obtained from the Lorentzian likelihood. Note that in both cases, we have scaled the amplitude power spectrum, A_s , by $\ln(10^{10} A_s)$ for clarity. The results are summarized in Table 1. The quoted values are the medians of the individual posterior distributions. The quoted errorbars represent the 16th and 84th percentiles, corresponding to the 68% confidence interval. Utilizing these results, we computed the best fit and the resulting residuals. The results obtained from the Gaussian likelihood yielded a reduced chi-square of $\chi_\nu^2 = 1.026$ whereas the Lorentzian likelihood yielded $\chi_\nu^2 = 1.027$.

	$\ln(10^{10} A_s)$	n_s	τ	$\Omega_b h^2$	$\Omega_c h^2$	$H_0 [\text{km s}^{-1} \text{Mpc}^{-1}]$
Gaussian	$3.08_{-0.5}^{+0.5}$	$0.969_{-0.006}^{+0.006}$	$0.08_{-0.03}^{+0.03}$	$0.0221_{-0.0001}^{+0.0001}$	$0.118_{-0.002}^{+0.002}$	67_{-1}^{+1}
Lorentzian	$3.10_{-0.06}^{+0.05}$	$0.973_{-0.008}^{+0.008}$	$0.09_{-0.03}^{+0.02}$	$0.0221_{-0.0001}^{+0.0001}$	$0.117_{-0.003}^{+0.003}$	69_{-1}^{+1}

Table 1. Results of MCMC. Quoted results are the median of the posterior distributions. Errorbars are given by the 16th and 84th percentiles, corresponding to the 68% confidence interval.

Given that both χ_ν^2 were both extremely close to 1, it is clear that both samplers were able to converge onto values for the model parameters, in agreement with one another within the 68% confidence interval. Across the board (with the exception of $\Omega_c h^2$), the Lorentzian model favoured slightly larger model parameters as opposed to the Gaussian model. Upon observation, Figure 4 highlights this clearly, and it appears that the posterior set by Pico is cutting off the posterior at larger values. Overall, however, the Gaussian and Lorentzian results are both extremely similar with the Gaussian likelihood being slightly favoured due to a slightly smaller value of χ_ν^2 . In both cases, we observe multiple correlations between various model parameters. For example, there exists a strong positive correlation between τ and A_s , a strong negative correlation between n_s and $\Omega_c h^2$ and seemingly no correlation between $\Omega_c h^2$ and A_s , to highlight a few. If given the opportunity, we would like to test a more realistic form of the likelihood and see if these correlations continue to appear. If so, this would provide an extremely strong tool for measuring the strength of the correlation between model parameters.

5. CONCLUSION

Although both the Gaussian and Lorentzian likelihoods cannot be the exact form of the likelihoods, we successfully demonstrated the constraint of six of the basic cosmological parameters using Markov

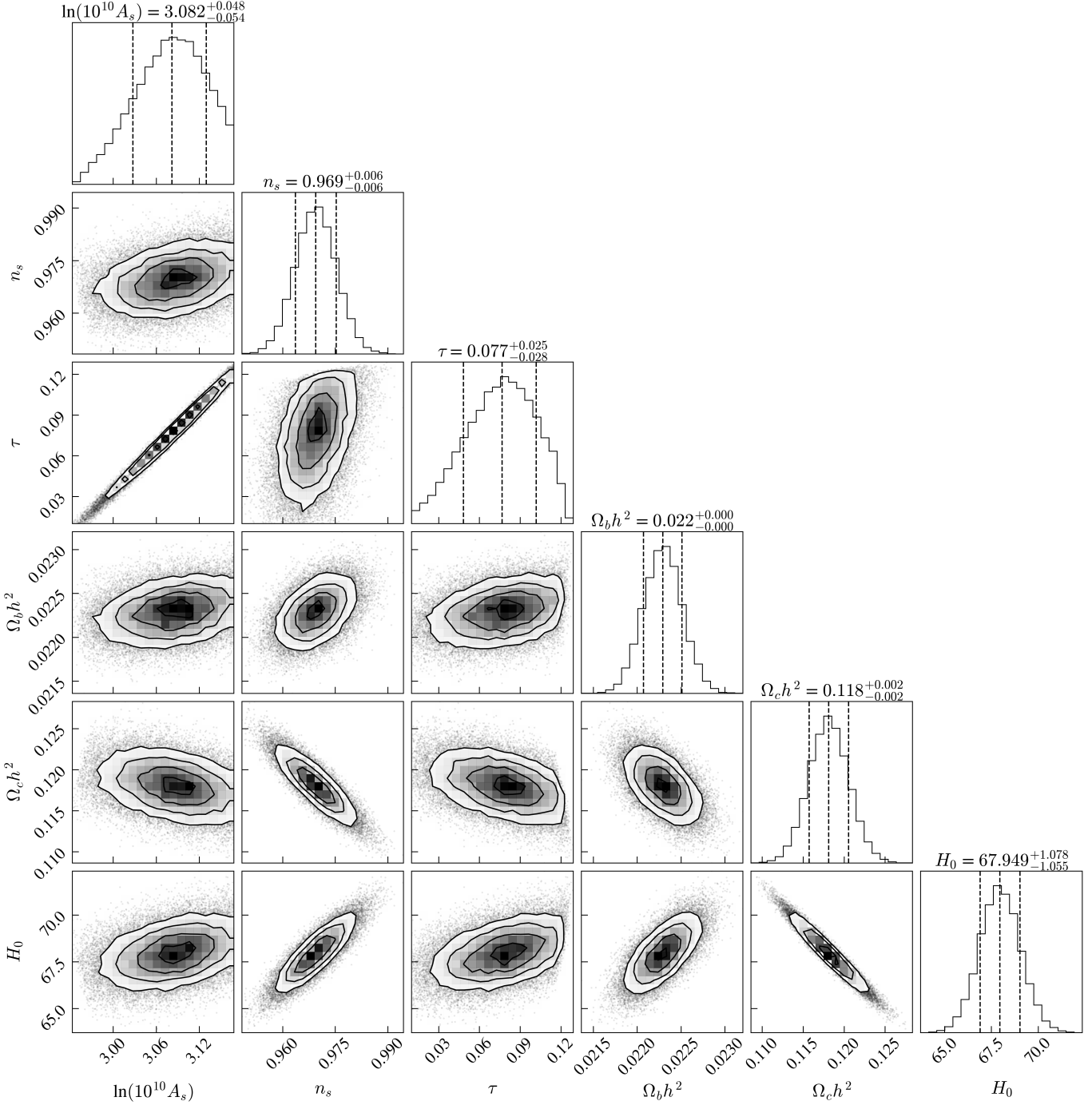


Figure 3. Posterior distributions of model parameters assuming a Gaussian likelihood. MCMC was sampled over 10,000 steps with 50 walkers using `emcee`. Median, 16th and 84th percentiles are indicated with the dashed lines. First 1000 steps were removed to neglect the burn in period.

Chain Monte Carlo analysis. This report further serves as a motivator towards the development of additional emulators such as Pico. While not perfect, much of the physics is contained within these emulators, allowing for quick confirmation and determination of the fundamental results that the true experiment would provide. As a whole, it acts as an excellent foundation before attempting to

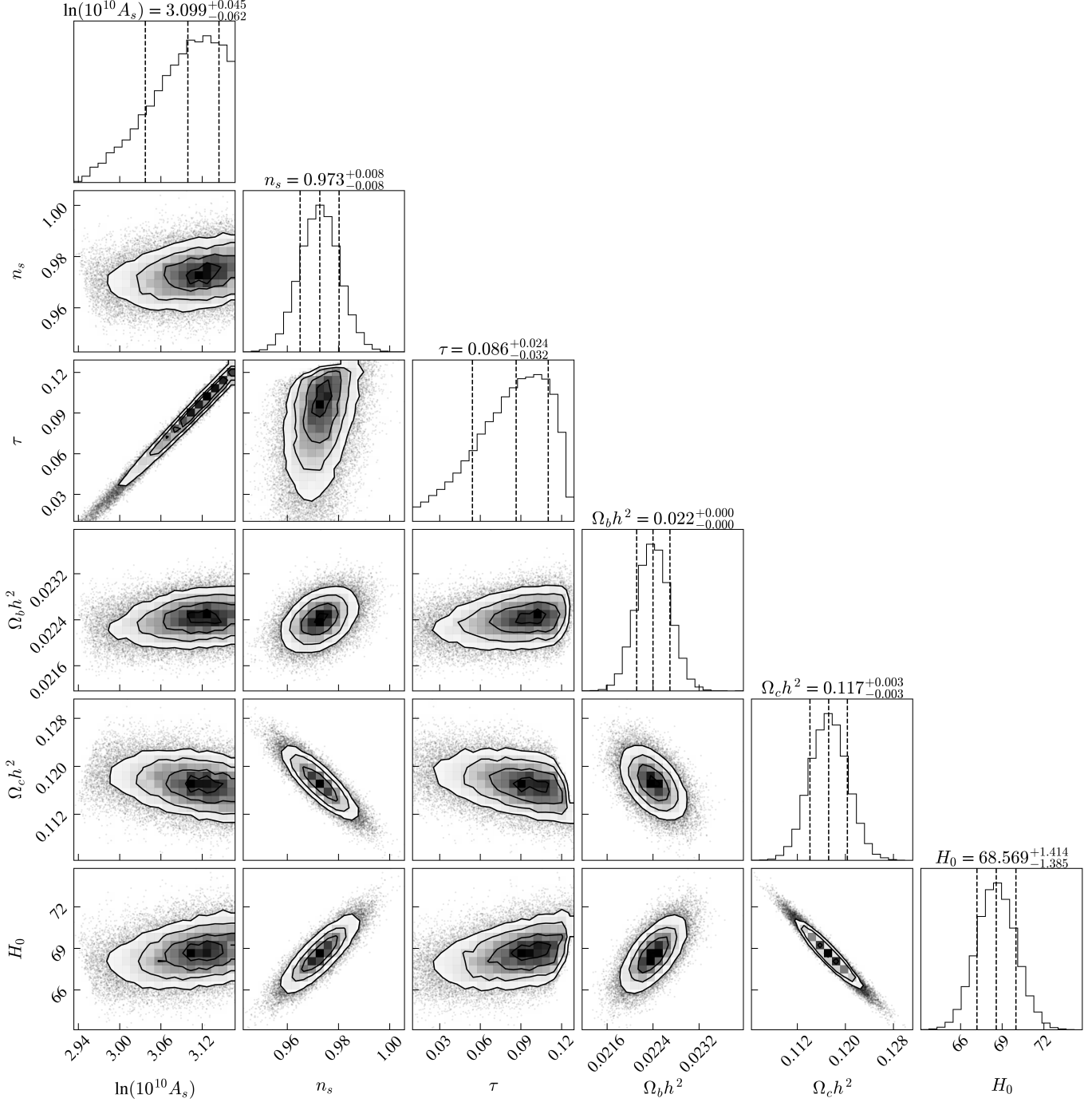


Figure 4. Posterior distributions of model parameters assuming a Lorentzian likelihood. MCMC was sampled over 10,000 steps with 50 walkers using `emcee`. Median, 16th and 84th percentiles are indicated with the dashed lines. First 1000 steps were removed to neglect the burn in period.

solve the entire problem using the most up-to-date software packages (which take increasingly long times to run!). We hope that this report serves as a reminder of the strength of MCMCs in their ability to constrain increasingly complex systems that govern our universe.

REFERENCES

- Fendt, W. A., & Wandelt, B. D. 2007, The Astrophysical Journal, 654, 2,
doi: [10.1086/508342](https://doi.org/10.1086/508342)
- Foreman-Mackey, D., Hogg, D. W., Lang, D., & Goodman, J. 2013, Publications of the Astronomical Society of the Pacific, 125, 306,
doi: [10.1086/670067](https://doi.org/10.1086/670067)
- Kramm, G., & Mölders, N. 2009, Planck's blackbody radiation law: Presentation in different domains and determination of the related dimensional constants, arXiv,
doi: [10.48550/ARXIV.0901.1863](https://arxiv.org/abs/0901.1863)
- Noterdaeme, P., Petitjean, P., Srianand, R., Ledoux, C., & Ló pez, S. 2011, Astronomy & Astrophysics, 526, L7,
doi: [10.1051/0004-6361/201016140](https://doi.org/10.1051/0004-6361/201016140)